

## Non-Hermitian Aharonov-Bohm effect in the quantum ring

Qingming Li,<sup>1</sup> Jian-Jun Liu,<sup>1,2,\*</sup> and Ying-Tao Zhang<sup>1,†</sup>

<sup>1</sup>College of Physics, Hebei Normal University, Shijiazhuang 050024, China

<sup>2</sup>Department of Physics, Shijiazhuang University, Shijiazhuang 050035, China

 (Received 15 September 2020; revised 11 December 2020; accepted 7 January 2021; published 15 January 2021)

We investigate the topological properties, energy spectrum, and persistent currents of a non-Hermitian ring with anti-Hermitian hopping terms. It is demonstrated that the anti-Hermitian hopping can effectively induce a synthetic gauge field. As the magnetic flux of the synthetic gauge field threads through the ring, the non-Hermitian system exhibits an Aharonov-Bohm effect. For the case of a non-Hermitian ring in the topological phase, the system, having an energy spectrum structure with a real gap, supports an imaginary persistent current. For the trivial case, a non-Hermitian system with an imaginary gap supports a real persistent current. Furthermore, we also investigate the transport property of a non-Hermitian Aharonov-Bohm ring connected by two semi-infinite leads. We find that the transmission coefficient shows the Aharonov-Bohm quantum oscillation as a function of the synthetic gauge field.

DOI: [10.1103/PhysRevB.103.035415](https://doi.org/10.1103/PhysRevB.103.035415)

### I. INTRODUCTION

There exist two routes when electrons are transported through a two-terminal quantum ring structure. As a magnetic field is applied perpendicular to the plane of such a ring, the electron wave function will acquire an extra phase. The extra phase coherence can give rise to quantum interference of electrons such as the well-known magnetic Aharonov-Bohm (AB) effect [1], which shows the eminent transport signal of the periodic oscillation as a function of magnetic flux [2–4]. Since AB oscillation was experimentally observed in the mesoscopic regime in metallic [5,6] and semiconductor rings [7,8], the AB effect has become a standard tool to quantitatively investigate the phase coherence and is expected to have potential applications in realizing quantum computational devices.

However, the electromagnetic potential is not a necessary condition for the AB effect. Nitta and co-workers have proposed that the spin-interference device, consisting of a ballistic AB ring connected by a gate electrode, works by Rashba spin-orbit coupling [9,10]. Because neutral particles are not influenced by electromagnetic fields, the quest for the nonmagnetic AB effect is to create a situation in which a neutral particle acquires a geometric phase as it travels along a closed contour [11]. The geometric phase for the photons can be synthesized by dynamical modulation of the dielectric constant [12,13], magneto-optical effects through a connection with Berry's curvature [14–16], and photon-phonon interactions [17].

Recently, it has been demonstrated that an imaginary magnetic flux can be generated by the nonreciprocal coupling in a ringlike structure [18–22], which induces a non-Hermitian AB

effect [23]. However, as an imaginary magnetic flux makes the Bloch wave function of the particle no longer keep a periodic phase, it is difficult to observe the transport signal of the periodic oscillations as a function of the imaginary magnetic flux. In this paper, we propose a non-Hermitian AB ring, in which the anti-Hermitian intradimer hopping is considered. It is found that a *real* magnetic flux can be induced by the anti-Hermitian interaction. As the magnetic flux threads the ring, the particles traveling around the ring will undergo a periodic phase shift, and the observable non-Hermitian AB effect will occur.

The rest of the paper is organized as follows. In Sec. II, we investigate the model Hamiltonian and the topological properties of the non-Hermitian system. In Sec. III, we study the band structure of the system under the periodic boundary condition (PBC). In Sec. IV, we investigate the persistent current of the non-Hermitian ring. In Sec. V, we calculate the transmission coefficient through a non-Hermitian AB ring, which shows the quantum AB oscillation as synthetic magnetic flux induced by anti-Hermitian hopping. Finally, a summary is presented in Sec. VI.

### II. MODEL AND TOPOLOGICAL PROPERTY

A typical one-dimensional tight-binding lattice with two sites per unit cell can be considered as an extension of the Su-Schrieffer-Heeger (SSH) lattices. The Hamiltonian for the extended SSH model under PBC with  $N$  pairs of lattice sites is given by

$$H = \sum_{j=1}^N (t_L c_{j,A}^\dagger c_{j,B} + t_R c_{j,B}^\dagger c_{j,A}) + \sum_{j=1}^{N-1} (t_2 c_{j,B}^\dagger c_{j+1,A} + \text{H.c.}) + (t_2 c_{N,B}^\dagger c_{1,A} + \text{H.c.}), \quad (1)$$

\*liujj@mail.hebtu.edu.cn

†zhangyt@mail.hebtu.edu.cn

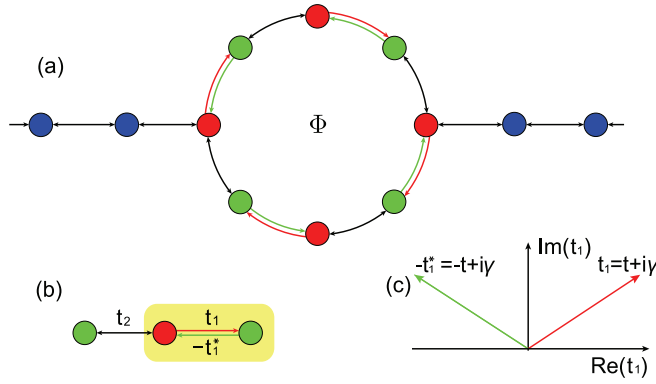


FIG. 1. (a) Schematic illustration of a non-Hermitian AB effect system. An array of dimeric lattices form a closed circle in the central scattering region. The nonzero magnetic flux threading the ring is induced by the anti-Hermitian coupling processes. The left and right terminals are exactly extended from unified lattices. (b) Detail of the tight-binding model of the asymmetric coupling processes.  $t_L = t_1$  and  $t_R = -t_1^*$  are intracell anti-Hermitian hopping terms which induce the Peierls phase, and  $t_2$  is the intercell hopping term. The yellow box indicates the unit cell. (c) The interaction between two adjacent lattices in the unit cell has an angle in the complex plane.

where  $t_L$  ( $t_R$ ) describes the intracell hopping from left to right (right to left) and  $t_2$  describes the intercell hopping.  $A$  and  $B$  describe the sublattice subspace. The index  $j$  denotes the number of the unit cell, and  $c_j^\dagger$  ( $c_j$ ) is the creation (annihilation) operator. Without loss of generality, we take the  $t_2$  in the second term of Eq. (1) to be real and positive. The last term, representing the hopping between two ends of the chain, implies that the system has PBC. We can approach the open boundary conduction (OBC) by removing the last term.

In Eq. (1), for  $t_L = t_R \in \mathbb{R}$ , the Hamiltonian describes the ordinary SSH model. For  $t_L \neq t_R \in \mathbb{R}$ , the Hamiltonian describes the SSH model with asymmetric intradimer hopping amplitudes, which has been proposed to produce the non-Hermitian skin effect [24–26]. The asymmetric hopping term leads to the breakdown of bulk-boundary correspondence [27,28], which is a guiding principle in the topological matter.

In this paper, our research mainly focuses on the case of the intracell hopping satisfying  $t_L = -t_R^* \in \mathbb{C}$ , which can be defined as the anti-Hermitian hopping. For more clarity, in Fig. 1(b) we show a schematic diagram of the intracell hopping terms  $t_L$  and  $t_R$  and the intercell hopping term  $t_2$ . While  $t_L$  can be described as  $t + i\gamma$ ,  $t_R$  will be set to  $-t + i\gamma$ , where both  $t$  and  $\gamma$  are the real numbers, as shown in Fig. 1(c). Here, we would like to point out that such anti-Hermitian hopping can be realized by an auxiliary cluster with dissipative sites coupled to the main network in optics [29].

In Figs. 2(a) and 2(b), we first plot the energy spectrum of the one-dimensional chain under PBC and OBC. It can be seen that the bulk states in the case of OBC do coincide with the bulk states for the system with PBC. However, there are two zero-energy modes in the energy spectrum of the system with OBC in Fig. 2(a). In Fig. 2(c), we calculate the distribution of the wave function along with the one-dimensional chain under OBC. One can see that the probability distribution of the wave function corresponding to the zero-energy modes is

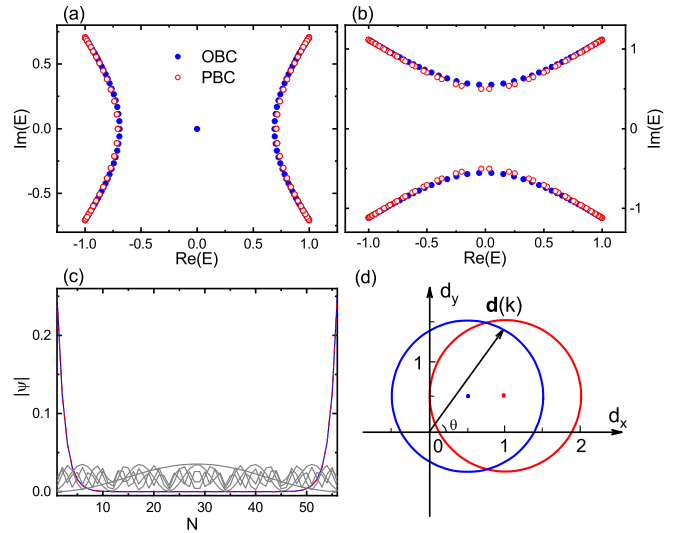


FIG. 2. Distribution of the energy spectrum in (a) the topological phase and (b) the trivial phase. The solid blue circles and the open red circles represent the eigenvalues of the non-Hermitian system under OBC and PBC, respectively. (c) Distribution of the eigenvectors on one-dimensional open chains. The blue and red lines show the wave functions of edge eigenvectors, and the remaining lines show the wave function of the bulk eigenvectors. (d) Geometric characterization of the non-Hermitian system. The parameters of the blue loop and the red loop correspond to the parameters in (a) and (b), respectively. The parameters are  $N = 56$ ,  $t = 0.5$ ,  $t_2 = 1$ , and (a)  $\gamma = 0.5$  and (b)  $\gamma = 1$ .

at the two boundaries and the wave functions of bulk states localize at the whole chain, which indicates the appearance of topological boundary states and that there is no skin effect. For a Hermitian SSH chain, the left and right edge modes are localized at both ends of the chain, respectively [30]. However, for our calculated non-Hermitian SSH chain with  $N = 56$ , the two boundary modes are simultaneously distributed at both ends of the chain.

In order to verify topological characterization of the non-Hermitian model, next we give the Hamiltonian in the momentum space

$$H(k) = (i\gamma + t_2 \cos k)\sigma_x + (it + t_2 \sin k)\sigma_y, \quad (2)$$

where  $\sigma_{x,y}$  are Pauli matrices. Now the topological invariant can be described by a winding number

$$w = \frac{1}{2\pi} \int_{-\pi}^{\pi} \partial_k \theta(k) dk, \quad (3)$$

where  $\theta(k) = \tan^{-1}(d_y/d_x)$  with  $d_y = it + t_2 \sin(k)$  and  $d_x = i\gamma + t_2 \cos(k)$ . The geometric characterization of the non-Hermitian system with the topological (trivial) phase is displayed in Fig. 2(d), where the blue (red) circle consists of the endpoints of the vector  $\mathbf{d}(k)$  as  $k$  goes across the Brillouin zone. Obviously, the winding number is determined by  $t_2$  and  $|t_1|$ , where  $|t_1| = \sqrt{t^2 + \gamma^2}$  is the distance from the center of the ring to the origin of the coordinates and  $t_2$  is the radius of the circle. Two different phases appear in the parameter space: a topological phase with the winding number  $w = 1$  for the case of  $|t_1| < t_2$  and a trivial phase with  $w = 0$  for

the case of  $|t_1| > t_2$ . In the topological phase, there exist two zero-energy states under OBC, the wave functions of which are localized at both ends of the non-Hermitian chain, as shown in Figs. 2(a) and 2(c).

Now it is clear that our proposed non-Hermitian model satisfies the bulk-boundary correspondence. Thus the non-Hermitian skin effect does not occur in such a non-Hermitian chain.

### III. NON-HERMITIAN AB RING

Now, let us concentrate on the non-Hermitian system under the PBC, where a key feature of the ring with anti-Hermitian hopping marks the presence of the AB effect. If we define the parameter  $\phi$  via  $t_L = t + i\gamma = |t_1|e^{i\phi}$ , the hopping terms are equivalent to a coupling amplitude  $|t_1| = \sqrt{t^2 + \gamma^2}$  with Peierls phase factor  $e^{i\phi}$ . In a similar way, we can define  $t_R = -t + i\gamma = -|t_1|e^{-i\phi}$ . When the phase factor accumulates along the circular path under the PBC, the total factor in one circle is  $e^{iN\phi}$ , where  $N$  is the number of unit cells. Thus the non-Hermitian system generates the real magnetic flux with a value of  $\Phi = N\phi$  in the ringlike structure (see Appendix A). The eigenvalues of Eq. (2) are

$$E_{\pm}(k, \phi) = \pm\sqrt{-|t_1|^2 + t_2^2 + 2i|t_1|t_2 \sin(k + \phi)}, \quad (4)$$

with  $k, \phi = 2\pi j/N$ , integer  $j \in [1, N]$ . From Eq. (4), one can see that the phase  $\phi$  and the wave vector  $k$  play the same role in the energy spectrum. It is easy to see that varying of  $\phi$  by  $2j\pi/N$  will get the same eigenvalue. Thus the magnetic flux  $\Phi$  can give rise to a periodic change in the complex plane of the energy spectrum. So it leads to a magneto-oscillation in the energy spectrum with an oscillation period of  $\Phi = 2\pi$ .

In order to observe this more intuitively, in Fig. 3 we plot the energy spectra as a function of the real magnetic flux  $\Phi$ , where  $|t_1| = t_2$ ,  $|t_1| > t_2$ , and  $|t_1| < t_2$  are considered in the non-Hermitian system, respectively, and  $|t_1| = t_2$  is considered in the Hermitian system. The following conclusions can be drawn.

(i) For  $|t_1| = t_2$ , the eigenvalues will be given by  $E_{\pm} = \pm\sqrt{-2i|t_1|t_2 \sin(k + \phi)}$ . In Fig. 3(a), it can be seen that the projection of eigenvalues lies on two straight lines  $\text{Re}(E) = \pm\text{Im}(E)$  in the complex-energy plane. While the magnetic flux  $\Phi$  is adjusted from  $-3\pi$  to  $3\pi$ , the complex-energy bands have evolved through three periods, which implies the presence of the non-Hermitian AB effect. Since such energy spectra are continuously distributed in both real and imaginary space in the complex-energy plane, the non-Hermitian system has a gapless band structure (see red lines in Fig. 3). Actually,  $|t_1| = t_2$  corresponds to the topological phase transition point between the trivial phase and the topological phase in the parameter space, and it can be seen in the discussion of Figs. 3(b) and 3(c) below that the gap band will be produced for  $|t_1| \neq t_2$ .

(ii) In Fig. 3(b), we show that the projection of the complex eigenvalue lies on a hyperbola in the complex-energy plane for the topological phase with the parameter relationship  $|t_1| < t_2$ . The reason for this is that the relationship between the real part and the imaginary part of the eigenvalue is given

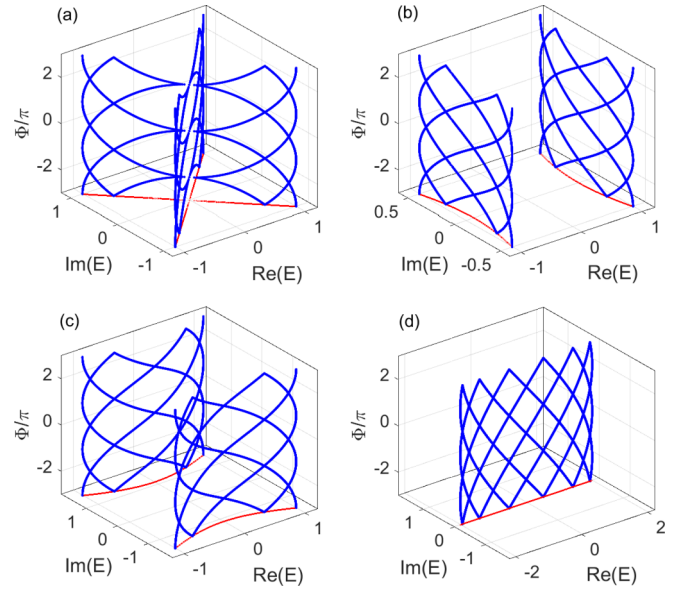


FIG. 3. Complex-energy spectra for the AB ring as functions of the real magnetic flux  $\Phi$ . The projections of the energy spectra onto the complex plane are also presented with red lines for a better view. The system parameters are  $N = 6$ ,  $t_2 = 1$ , and (a)  $|t_1| = 1$ , (b)  $|t_1| = 0.5$ , (c)  $|t_1| = 1.5$ , and (d)  $t_1 = 1$ .

by

$$[\text{Re}(E)]^2 - [\text{Im}(E)]^2 = t_2^2 - |t_1|^2, \quad (5)$$

where  $\text{Re}(E)$  and  $\text{Im}(E)$  satisfy the equation of a hyperbola. From Fig. 3(b), one can see that the projections of two continuous parts of the band spectrum on the complex-energy plane neither touch nor intersect for any  $\Phi$ , so there exists a line gap in the band spectrum (see the red lines) [31]. In Refs. [31,32], it was shown that if an energy spectrum of the non-Hermitian Hamiltonian has a line gap, it could be continuously flattened into a Hermitian Hamiltonian with a real gap or an anti-Hermitian Hamiltonian with an imaginary gap. Based on the above point of view, the flattening procedures in our model can be accomplished by gradually reducing the value of  $|t_1|$ . For  $|t_1| = 0$ , the anti-Hermitian intradimer hopping terms vanish, and Eq. (2) is transformed into a Hermitian Hamiltonian with the eigenvalues  $\pm t_2$ . Thus, for the topological phase with  $|t_1| < t_2$  in our model, the non-Hermitian ring hosts a real gap with the magnitude  $\{-t_2, t_2\}$ . Besides, as the magnetic flux  $\Phi$  varies, the energy spectrum shows a periodic change with an oscillation period of  $\Phi = 2\pi$ , which means that the non-Hermitian AB effect should be produced.

(iii) In Fig. 3(c), we also show that the energy spectrum generates periodic oscillation by magnetic flux  $\Phi$  for the trivial phase with  $|t_1| > t_2$ . From Eq. (5), it is easy to verify that the projection of two continuous parts of the spectrum lies on a hyperbola in the complex-energy plane with its focal points located at the real axis. Similar to the flattening procedures mentioned earlier, when the value of  $t_2$  gradually decreases to zero through adiabatic approximation, the Hermitian inter-dimer hopping terms vanish. At this time, the non-Hermitian Hamiltonian in Eq. (2) is transformed into an anti-Hermitian

Hamiltonian with the imaginary eigenvalues  $\pm i|t_1|$ . Thus the magnitude of an imaginary gap is  $\{-i|t_1|, i|t_1|\}$ .

(iv) Last, we briefly discuss the physical property of the Hermitian Hamiltonian. The purpose of introducing the Hermitian model is to compare with the non-Hermitian model, in order to provide the similarities and differences between the two models. The intracell hopping terms of the Hermitian system are  $t_L = t_1 = t + i\gamma$  and  $t_R = t_1^* = t - i\gamma$ , which symmetrically distribute about the real coordinate axis of  $t_1$ . The Bloch Hamiltonian of the Hermitian system is

$$H_{\text{Her}}(k) = (t + t_2 \cos k)\sigma_x + (\gamma + t_2 \sin k)\sigma_y, \quad (6)$$

where  $\gamma$  is an extensional term of the general SSH model. Through a similar transformation which we have mentioned earlier, we can rewrite the intracell hopping as  $t_1 = |t_1|e^{i\phi}$ . The energy dispersion relation of Eq. (6) reads

$$E_{\text{Her},\pm}(k) = \pm \sqrt{|t_1|^2 + t_2^2 + 2|t_1|t_2 \cos(k + \phi)}, \quad (7)$$

with  $k, \phi = \pi j/N$ , integer  $j \in [1, 2N]$ . The energy spectrum of the Hermitian system is exhibited in Fig. 3(d) for the case of  $t_1 = t_2$ .

#### IV. PERSISTENT CURRENTS

One of the well-known manifestations of the AB effect consists of the periodically nondissipative persistent currents in the ring threaded by a magnetic flux  $\Phi$ . In this section, we investigate the persistent current  $I(\Phi)$  as a function of the flux  $\Phi$  of our proposed non-Hermitian ring. The persistent current can be defined as

$$I(\Phi) = -c \frac{\partial E}{\partial \Phi}, \quad (8)$$

which indicates the derivative of the ground-state energy with respect to the magnetic flux [33,34]. Since the eigenvalues are distributed in the complex-energy plane for our proposed non-Hermitian system, the imaginary part of the current will be yielded [18,19].

For a ring with anti-Hermitian intradimer hopping in one unit cell, a current of the single state can be calculated as the derivative,

$$I_n(\Phi) = -c \frac{\partial E_n}{\partial \Phi} = -\frac{iI_0 t_1 \cos \phi_n}{\sqrt{t_2^2 - t_1^2 + 2t_1 t_2 i \sin \phi_n}}, \quad (9)$$

where  $\phi_n = \frac{1}{N}(2\pi n + \Phi)$ . The details of the calculations in Eq. (9) are presented in Appendix B. The total persistent current is obtained by the sum of the currents of all occupied electron states

$$I(\Phi) = \sum_{\text{occ}, n} I_n(\Phi). \quad (10)$$

For the case of  $|t_1| = t_2$ , Eq. (9) can be simplified to  $I_n = I_0 i t_1 \cos \phi_n / \sqrt{2t_1 t_2 i \sin \phi_n}$ , which implies that the persistent current is a straight line  $\text{Re}(I) = \text{Im}(I)$  in the complex plane. In Fig. 4(a), we plot the persistent current as a function of  $\Phi$  for the case of  $|t_1| = t_2$ . One can see that the persistent current is a  $2\pi$ -periodic function of  $\Phi$ . However, the function is not defined at  $\Phi = 2n\pi$ , corresponding to a removable discontinuity at this point in Fig. 4(a). The physical reason

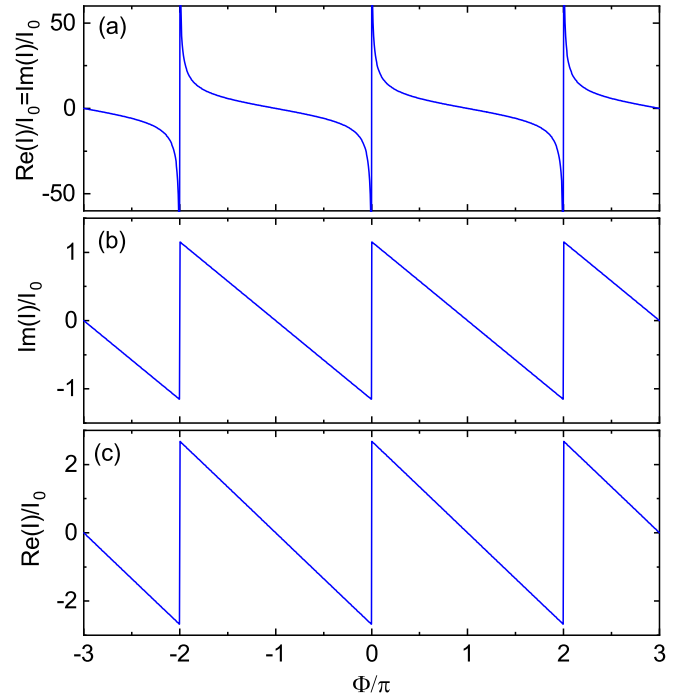


FIG. 4. Dimensionless persistent currents for the AB ring as functions of the magnetic flux  $\Phi$ . The current-flux relation  $I/I_0(\Phi)$  is exhibited in (a) the  $(I_{\text{Re}(I)=\text{Im}(I)}, \Phi)$  plane, (b) the  $(I_{\text{Re}(I)=0}, \Phi)$  plane, and (c) the  $(I_{\text{Im}(I)=0}, \Phi)$  plane. The system parameters are  $N = 60$ ,  $t_2 = 1$ , and (a)  $|t_1| = 1$ , (b)  $|t_1| = 0.5$ , and (c)  $|t_1| = 1.5$ .

is that the energy bands around  $E = 0$  are almost parallel to the complex plane of energy, as shown in Fig. 3(a). Thus the derivative of energy with respect to  $\Phi$  tends to infinity.

For the topological phase with  $|t_1| < t_2$ , in the non-Hermitian system there exists a real energy band gap. Since the real part of the energy band is discontinuous, the real persistent current cannot be produced in this case. However, as shown in Fig. 3(b), the imaginary part of the energy bands is continuous with the magnetic flux  $\Phi$ . Thus we can calculate an imaginary persistent current as a function of  $\Phi$ , as shown in Fig. 4(b). One can see that the imaginary persistent current also is a periodic function with period  $2\pi$  and exhibits discontinuous steps at  $\Phi = 2n\pi$ . The reason for this is that a single energy band passes through the imaginary Fermi surface  $\text{Im}(E) = 0$ , as shown in Fig. 3(b), which leads to the current reversal. In addition, we can get a similar conclusion by analyzing Eq. (9). While the number of unit cells  $N$  is large enough in the non-Hermitian ring, the persistent current of a single state is approximately expressed as  $I_n = iI_0 t_1 / \sqrt{t_2^2 - t_1^2}$ . For  $|t_1| < t_2$ , the denominator of the above formula is a real number, and the system supports an imaginary current.

For the case of  $|t_1| > t_2$ , the system is a trivial phase, and in this case the energy band hosts an imaginary gap. According to the above analysis, we know that only the real persistent current could be produced by the magnetic flux  $\Phi$ , which is plotted in Fig. 4(c). We can see that the real persistent current also is a periodic function with period  $2\pi$  and exhibits discontinuous steps at  $\Phi = 2n\pi$ , for the same reasons as in the case of the topological phase.

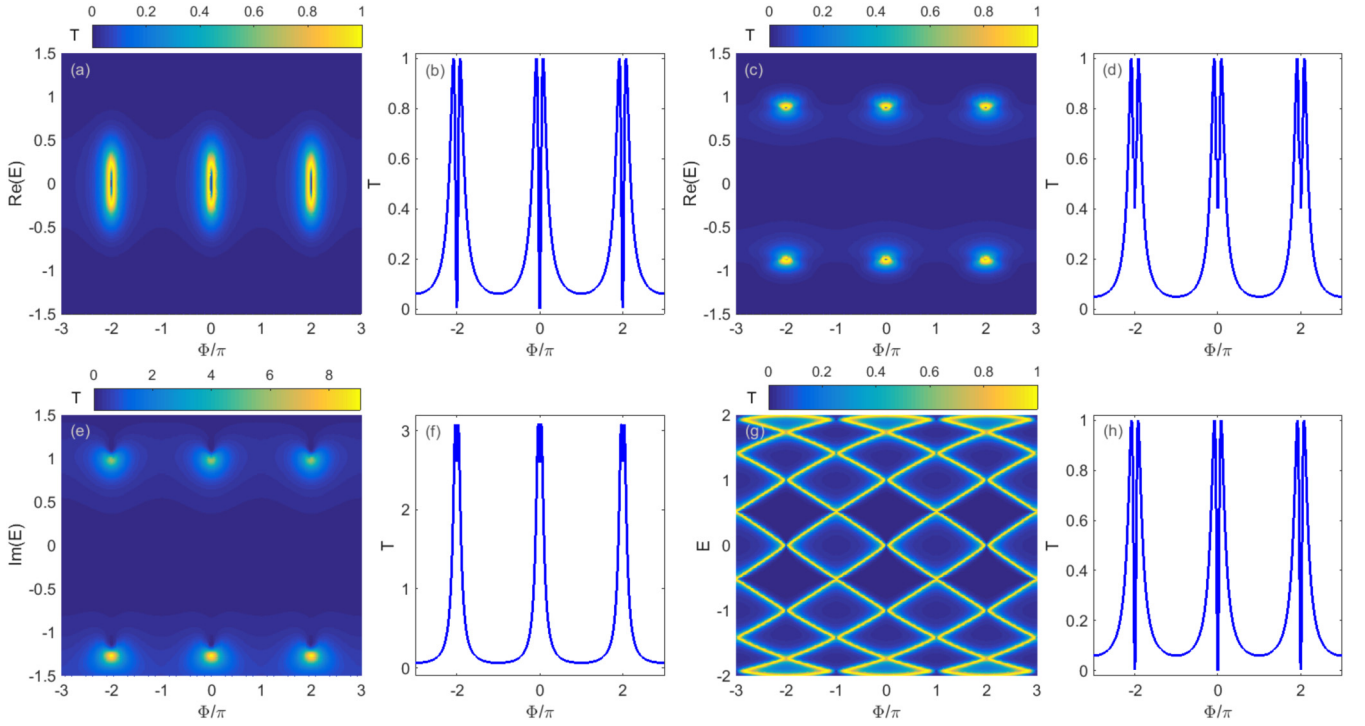


FIG. 5. (a), (c), (e), and (g) The transmission coefficient  $T$  as a function of the Fermi energy  $E$  and the magnetic flux  $\Phi$ . (b), (d), (f), and (h) The transmission coefficient  $T$  as a function of the magnetic flux  $\Phi$  with the fixed Fermi energy  $E = 0$  for (b) and (h),  $E = 0.86$  for (d), and  $E = 1.15i$  for (f). The coupling amplitude of intracell anti-Hermitian hopping is  $|t_1| = 1$  for (a) and (b),  $|t_1| = 0.5$  for (c) and (d), and  $|t_1| = 1.5$  for (e) and (f). The coupling amplitude of intracell Hermitian hopping is  $|t_1| = 1$  for (g) and (h). The other system parameters are  $N = 6$  and  $t_2 = 1$ . The coupling term between the left (right) terminal and the central scattering region is set to 0.4.

Recently, we have also noticed that the persistent current is predicted in the non-Hermitian ring in Ref. [35], in which the non-Hermitian skin effect is also related to the persistent current. In our model, the persistent current is not completely related to the non-Hermitian skin effect.

## V. NON-HERMITIAN AB OSCILLATION

From the view of the band spectrum, we have predicted that the non-Hermitian AB effect could be produced in our proposal anti-Hermitian quantum ring system. To verify the existence of the non-Hermitian AB effect in more detail, we investigate the electron transmission through the non-Hermitian quantum ring doubly connected systems [see Fig. 1(a)] by using the nonequilibrium Green's function method [36–38]. Assuming that there is an incoming electron with energy  $E$  from the left terminal and transport through the non-Hermitian AB ring, the transmission coefficient  $T$  can be written as [39]

$$T(E, \Phi) = \text{Tr}[\Gamma^L(E)G^r(E, \Phi)\Gamma^R(E)G^a(E, \Phi)], \quad (11)$$

where  $\Gamma^L(E) = i[\Sigma_L^r - \Sigma_L^a]$  and  $\Gamma^R(E) = i[\Sigma_R^r - \Sigma_R^a]$  are the linewidth functions.  $\Sigma_L^r = \Sigma_L^{a,\dagger} = H_{LC}g^r H_{CL}$  ( $\Sigma_R^r = H_{RC}g^r H_{CR}$ ) is the retarded self-energy contributed by the left (right) semi-infinite lead [40].  $H_{LC}$  ( $H_{RC}$ ) is the coupling term between the left (right) terminal and the central scattering region, and  $g^r$  is the surface Green's function of the semi-infinite lead. In Eq. (11),  $G^r = [G^a]^\dagger = (E - H_C - \Sigma_L^r - \Sigma_R^r)^{-1}$  is

the retarded Green's function of the central scattering region, where  $H_C$  is the tight-binding Hamiltonian of the AB ring and  $E$  is the Fermi energy.

In Fig. 5(a), at fixed parameters  $|t_1| = t_2 = 1$ , we plot the transmission coefficient  $T$  as a function of the Fermi energy  $E$  and the magnetic flux  $\Phi$ . One can see that the electron transmission coefficient has three peak regions in the plane which consists of the real Fermi energy  $E$  and the magnetic flux  $\Phi$ . In Fig. 3(a), we showed that the coalescing points of two bands emerge at the fixed parameters  $E = 0$  and  $\Phi = 2j\pi$  while the Fermi energy changes in the real-valued range. The peak regions of the transmission coefficient almost correspond to the three coalescing points of the two bands. However, in Fig. 5(a), one can see that the destructive interference with tunneling coefficient  $T = 0$  appears at  $\Phi = 2j\pi$  and  $E = 0$ , and constructive interference with tunneling coefficient  $T = 1$  emerges near  $\Phi = 2j\pi$ . This abnormal phenomenon is because when we calculate the transport coefficient, two semi-infinite leads are connected on the ring, which change the structure of the system. Thus the smaller the hopping between the non-Hermitian ring and the lead, the closer the contour of the transport result is to the contour of the energy band. While the Fermi energy  $E = 0$  is fixed, the transmission coefficient shows the periodic oscillation as a function of the magnetic flux  $\Phi$ , as shown in Fig. 5(b), which indicates the occurrence of the non-Hermitian AB effect. In addition, for the case of  $\Phi \neq 2j\pi$ , the transport results show that even when the Fermi energy is zero, the non-Hermitian ring still has a transport coefficient,

which indicates that the system supports the persistent current.

In Fig. 5(c), the transmission coefficient is plotted with the fixed parameters  $|t_1| = 0.5$  and  $t_2 = 1$ . In Fig. 3(b), we demonstrated that the gap between conduction and valence bands will be produced for  $|t_1| < t_2$ . In Fig. 5(c) it can be found that the transmission coefficient shows zero value while the Fermi energy  $E_F$  is zero, and the peaks of the transmission coefficient with the value of  $T = 1$  occur for  $E = \pm\sqrt{t_2^2 - |t_1|^2}$  and  $\Phi = 2j\pi$ . The reason for this is that while the Fermi energy changes in the real-valued range, the real-valued bands of the energy spectrum emerge in  $E = \pm\sqrt{t_2^2 - |t_1|^2}$  and  $\Phi = 2j\pi$ , as shown in Fig. 3(b). Besides, in Fig. 5(d) one can see that the transmission coefficients show the periodic oscillation as a function of the magnetic flux  $\Phi$  for the Fermi energy  $E = 0.86$ . Thus we can observe the transport signal of the AB oscillations with a period of  $2\pi$  in this case.

Since the non-Hermitian system hosts an imaginary gap for the case of  $|t_1| > t_2$ , the variation of the Fermi energy in the real-valued range cannot obtain any transmission signal. To describe the transport properties of the non-Hermitian ring with an imaginary gap, we change the Fermi energy of the non-Hermitian quantum ring to the imaginary value Fermi energy, while we fix the incident energy as zero in the left and right leads. The transmission coefficient as a function of the imaginary-valued Fermi energy  $E$  and the magnetic flux  $\Phi$  is plotted in Fig. 5(e). It is worth noting that the transmission coefficient exceeds 1, which implies that the probability current is not conserved in the non-Hermitian AB ring. This behavior is because when we consider the incoming energy  $E$  to be imaginary valued in the calculation, it is equivalent to introducing gain or loss in the on-site term of the Hamiltonian. In general, the real value Fermi energy, referring to the energy difference between the highest and lowest occupied single-particle states, determines the average particle density in a quantum system of noninteracting fermions at absolute zero temperature. Through the above analysis, the complex Fermi energy can be understood as the average particle density in the system with gain or loss. This means that there is an exchange of particles or energy between the system and the external environment. Even so, one can see that the transmission peak corresponds well to the point where the energy spectrum intersects the imaginary axis in the complex plane, as shown in Fig. 3(c). Figure 5(f) shows the transmission coefficient as a function of the magnetic flux  $\Phi$  with the energy  $E = 1.15i$ . From Figs. 5(g) and 5(h), one can see that the non-Hermitian setup yields periodic oscillations.

Here, we briefly discuss the transport property when the non-Hermitian Hamiltonian in the central scattering region transforms into the Hermitian Hamiltonian. For the case of  $|t_1| = t_2 = 1$ , one can see that the peaks of the transmission coefficient, as shown in Fig. 5(g), can correspond well to the energy spectra, as shown in Fig. 3(d). In particular, for an incoming electron where the energy is  $E = 0$  and the hopping parameters satisfy the relationship  $|t_1| = t_2$ , the transport result of the Hermitian system is consistent with that of the non-Hermitian system, as shown in

Figs. 5(b) and 5(h). Similar conclusions have been mentioned in Refs. [41,42], in which they have investigated the Hermitian-like scattering behavior of a non-Hermitian scattering center with the anti-Hermitian hopping terms. In contrast to other non-Hermitian systems with dissipation and unconserved transmission probability, e.g., a system induced by hopping terms with amplifying or attenuating amplitude or a system with gain or loss, a system with anti-Hermitian hopping terms may exhibit a physical and conserved transport result. Thus a clear non-Hermitian AB oscillation is observed for the varying parameter relationship between  $|t_1|$  and  $t_2$ , as shown in Fig. 5.

## VI. CONCLUSION

We investigate the topological properties, energy spectrum, and persistent currents of a non-Hermitian ring with the anti-Hermitian hopping terms. An intercell anti-Hermitian hopping with complex values not only can supply the non-Hermiticity in the ringlike system but also can induce a phase factor. When the phase factor accumulates along the circular path under the PBC, the non-Hermitian system generates a synthetic gauge field thread through the ringlike structure, which leads to the non-Hermitian AB effect. The energy spectrum of the non-Hermitian AB ring holds the periodicity by the synthetic magnetic flux and exhibits the hyperbola in the complex-energy plane. The hyperbolic spectrum hosts a real gap in the topological phase or an imaginary gap in the trivial phase, which can be controlled by the parameters of appropriate hopping terms in the model. For the topological phase, the non-Hermitian ring supports an imaginary persistent current; for the trivial phase, the system supports a real persistent current. To further verify the AB effect in the non-Hermitian system, we investigate the electron transmission through a system which is composed of a non-Hermitian ring and two semi-infinite one-dimensional leads. Our transport results can support the AB oscillations and provide an effective demonstration of the presence of the real (imaginary) gap in the ringlike system.

## ACKNOWLEDGMENTS

This work was financially supported by the National Natural Science Foundation of China (Grants No. 11474084 and No. 12074097) and the Natural Science Foundation of Hebei Province (Grant No. A2020205013).

## APPENDIX A: PEIERLS PHASE FACTORS

In this Appendix, we give a simple derivation of the Peierls substitution. The Peierls substitution method gives a very convincing way of taking the complex-valued anti-Hermitian hopping as a synthetic gauge field. The Hamiltonian of a one-dimensional tight-binding lattice with an anti-Hermitian hopping is given by

$$H = \sum_{j=1}^N [(t + i\gamma)c_j^\dagger c_{j+a} + (-t + i\gamma)c_{j+a}^\dagger c_j] \\ = \sum_{j=1}^N (|t_1|e^{i\phi}c_j^\dagger c_{j+a} - |t_1|e^{-i\phi}c_{j+a}^\dagger c_j), \quad (\text{A1})$$

where  $a$  describes the lattice constant. Through the Fourier transformation, the creation and annihilation operators can be described as

$$c_j^\dagger = \frac{1}{\sqrt{Na}} \sum_k e^{-ikr_j} c_k^\dagger, \quad (\text{A2})$$

$$c_j = \frac{1}{\sqrt{Na}} \sum_k e^{ikr_j} c_k. \quad (\text{A3})$$

Under this representation, it is easy to get  $c_{j+a}^\dagger c_j = e^{-ip_x a/\hbar} c_j^\dagger c_j$ , where the momentum satisfies  $p_x = \hbar k$ . Because the vector potential does not vary significantly over one lattice spacing, we can set the phase factors to  $\phi = \frac{aqA_x}{\hbar}$  and expand up to the second order the phase factors by  $e^{i\phi} = 1 + \frac{iaqA_x}{\hbar} - \frac{a^2 q^2 A_x^2}{2\hbar^2} + \mathcal{O}(a^3)$ . Substituting these expansions into the relevant part of the Hamiltonian yields

$$\begin{aligned} H_j &= e^{i\phi} c_{j+a}^\dagger c_j - e^{-i\phi} c_{j+a}^\dagger c_j \\ &= \left[ 1 + \frac{iaqA_x}{\hbar} - \frac{a^2 q^2 A_x^2}{2\hbar^2} + \mathcal{O}(a^3) \right] \\ &\quad \times \left[ 1 - \frac{ip_x a}{\hbar} - \frac{p_x^2 a^2}{2\hbar^2} + \mathcal{O}(a^3) \right] c_j^\dagger c_j \\ &\quad - \left[ 1 - \frac{iaqA_x}{\hbar} - \frac{a^2 q^2 A_x^2}{2\hbar^2} + \mathcal{O}(a^3) \right] \\ &\quad \times \left[ 1 + \frac{ip_x a}{\hbar} - \frac{p_x^2 a^2}{2\hbar^2} + \mathcal{O}(a^3) \right] c_j^\dagger c_j \\ &= i \frac{2a}{\hbar} (p_x - qA_x) c_j^\dagger c_j. \end{aligned} \quad (\text{A4})$$

Then, we arrive at the Hamiltonian at the continuum limit,

$$H = i \frac{2a}{\hbar} (p - qA). \quad (\text{A5})$$

Note that the reason for the unit imaginary number in Eq. (A5) is that the Hamiltonian is an anti-Hermitian matrix with an imaginary eigenvalue. Hence an anti-Hermitian hopping term is equivalent to the hopping terms subjected to a synthetic magnetic field.

## APPENDIX B: PERSISTENT CURRENT

In this Appendix, we provide a detailed derivation of the persistent current for the single energy state in Eq. (9). For a quantum ring system with the anti-Hermitian intradimer

hopping  $t_L = -t_R^* \in \mathbb{C}$ , the tight-binding Hamiltonian is given by Eq. (A1), in which  $\phi$  is the corresponding phase change from unit cell  $j$  to  $j + 1$ ,

$$\phi = \frac{e}{c\hbar} \int_j^{j+1} \mathbf{A} \cdot d\mathbf{l} = \frac{2\pi\Phi}{N\Phi_0}, \quad (\text{B1})$$

where  $\Phi_0$  is the magnetic flux quantum. From the PBC, we can obtain  $\psi_L = \psi_0 e^{i2\pi\Phi/\Phi_0} = \psi_0 e^{i2n\pi}$ , where  $L$  is the circumference of the ring and  $n = 0, \pm 1, \pm 2, \dots$  is an integer. Then the wave function of the  $j$ th unit cell can be expressed as  $\psi_j = \psi_0 e^{i\frac{j}{N}2n\pi}$ , and one can obtain the relationship between the wave function of two adjacent unit cells

$$\psi_{j+1} = \psi_j e^{i\frac{2n\pi}{N}}. \quad (\text{B2})$$

Substituting this wave function into the Schrödinger equation  $H|\psi\rangle = E|\psi\rangle$ , we can obtain

$$\begin{aligned} \begin{pmatrix} 0 & |t_1| e^{-i\frac{2\pi}{N}(\frac{\Phi}{\Phi_0})} \\ 0 & 0 \end{pmatrix} \begin{pmatrix} \psi_{j,A} \\ \psi_{j,B} \end{pmatrix} e^{-i\frac{2n\pi}{N}} + \begin{pmatrix} -E & t_2 \\ t_2 & -E \end{pmatrix} \\ \times \begin{pmatrix} \psi_{j,A} \\ \psi_{j,B} \end{pmatrix} + \begin{pmatrix} 0 & 0 \\ -|t_1| e^{i\frac{2\pi}{N}(\frac{\Phi}{\Phi_0})} & 0 \end{pmatrix} \begin{pmatrix} \psi_{j,A} \\ \psi_{j,B} \end{pmatrix} e^{i\frac{2n\pi}{N}} = 0. \end{aligned} \quad (\text{B3})$$

Then the energy eigenvalues of the  $n$ th energy level can be obtained:

$$E_n = \pm \sqrt{t_2^2 - |t_1|^2 + 2|t_1|t_2 i \sin\left[\frac{2\pi}{N}\left(n + \frac{\Phi}{\Phi_0}\right)\right]}. \quad (\text{B4})$$

At the zero temperature, the persistent current is defined as the derivative of the ground-state energy  $I(\Phi) = -c\partial E/\partial\Phi$ , which for a single energy state has the form

$$I_n(\Phi) = \frac{-2\pi c i |t_1| t_2 \cos\left[\frac{2\pi}{N}\left(n + \frac{\Phi}{\Phi_0}\right)\right]}{N\Phi_0 \sqrt{t_2^2 - |t_1|^2 + 2|t_1|t_2 i \sin\left[\frac{2\pi}{N}\left(n + \frac{\Phi}{\Phi_0}\right)\right]}. \quad (\text{B5})$$

Defining the current amplitude as  $I_0 = 2\pi c t_2 / N\Phi_0$ , finally we can obtain Eq. (9).

It is worth noting that the total persistent current is given by the sum of the currents of all occupied electron states. Since the eigenvalues of the non-Hermitian system are distributed on the complex-energy plane, it is natural to define the Fermi surfaces occupying the real or imaginary energy levels, respectively, and we can obtain the the real (imaginary) part of the persistent current.

[1] Y. Aharonov and D. Bohm, *Phys. Rev.* **115**, 485 (1959).

[2] F. Bloch, *Phys. Rev.* **166**, 415 (1968).

[3] N. Byers and C. N. Yang, *Phys. Rev. Lett.* **7**, 46 (1961).

[4] Y. Gefen, Y. Imry, and M. Ya. Azbel, *Phys. Rev. Lett.* **52**, 129 (1984).

[5] L. P. Levy, G. Dolan, J. Dunsmuir, and H. Bouchiat, *Phys. Rev. Lett.* **64**, 2074 (1990).

[6] V. Chandrasekhar, R. A. Webb, M. J. Brady, M. B. Ketchen, W. J. Gallagher, and A. Kleinsasser, *Phys. Rev. Lett.* **67**, 3578 (1991).

[7] D. Mailly, C. Chapelier, and A. Benoit, *Phys. Rev. Lett.* **70**, 2020 (1993).

[8] A. Fuhrerl, S. Lüscherl, T. Ihn, T. Heinzel, K. Ensslin, W. Wegscheider, and M. Bichler, *Nature (London)* **413**, 822 (2001).

[9] J. Nitta, F. E. Meijer, and H. Takayanagi, *Appl. Phys. Lett.* **75**, 695 (1999).

[10] J. Nitta and T. Koga, *J. Supercond.* **16**, 689 (2003).

[11] J. Dalibard, F. Gerbier, G. Juzeliūnas, and P. Öhberg, *Rev. Mod. Phys.* **83**, 1523 (2011).

- [12] K. Fang, Z. Yu, and S. Fan, *Nat. Photonics* **6**, 782 (2012).
- [13] K. Fang, Z. Yu, and S. Fan, *Phys. Rev. Lett.* **108**, 153901 (2012).
- [14] F. D. M. Haldane and S. Raghu, *Phys. Rev. Lett.* **100**, 013904 (2008).
- [15] K. Fang, Z. Yu, and S. Fan, *Phys. Rev. B* **84**, 075477 (2011).
- [16] Z. Yu, G. Veronis, Z. Wang, and S. Fan, *Phys. Rev. Lett.* **100**, 023902 (2008).
- [17] E. Li, B. J. Eggleton, K. Fang, and S. Fan, *Nat. Commun.* **5**, 3225 (2014).
- [18] N. Hatano and D. R. Nelson, *Phys. Rev. Lett.* **77**, 570 (1996).
- [19] N. Hatano and D. R. Nelson, *Phys. Rev. B* **56**, 8651 (1997).
- [20] S. Longhi, D. Gatti, and G. Della Valle, *Sci. Rep.* **5**, 13376 (2015).
- [21] S. Longhi, *Phys. Rev. A* **92**, 042116 (2015).
- [22] A. McDonald, T. Pereg-Barnea, and A. A. Clerk, *Phys. Rev. X* **8**, 041031 (2018).
- [23] L. Jin and Z. Song, *Phys. Rev. B* **99**, 081103(R) (2019).
- [24] S. Yao and Z. Wang, *Phys. Rev. Lett.* **121**, 086803 (2018).
- [25] C. H. Lee and R. Thomale, *Phys. Rev. B* **99**, 201103(R) (2019).
- [26] K. Yokomizo and S. Murakami, *Phys. Rev. Lett.* **123**, 066404 (2019).
- [27] Y. Xiong, *J. Phys. Commun.* **2**, 035043 (2018).
- [28] F. K. Kunst, E. Edvardsson, J. C. Budich, and E. J. Bergholtz, *Phys. Rev. Lett.* **121**, 026808 (2018).
- [29] S. Longhi, *Phys. Rev. A* **93**, 022102 (2016).
- [30] J. K. Asbóth, L. Oroszlány, and A. Pályi, *A Short Course on Topological Insulators: Band Structure and Edge States in One and Two Dimensions*, Lecture Notes in Physics Vol. 919 (Springer International, Cham, Switzerland, 2016).
- [31] K. Kawabata, S. Higashikawa, Z. Gong, Y. Ashida, and M. Ueda, *Nat. Commun.* **10**, 297 (2019).
- [32] K. Kawabata, K. Shiozaki, M. Ueda, and M. Sato, *Phys. Rev. X* **9**, 041015 (2019).
- [33] H.-F. Cheung, Y. Gefen, E. K. Riedel, and W.-H. Shih, *Phys. Rev. B* **37**, 6050 (1988).
- [34] K. A. Matveev, A. I. Larkin, and L. I. Glazman, *Phys. Rev. Lett.* **89**, 096802 (2002).
- [35] K. Zhang, Z. Yang, and C. Fang, *Phys. Rev. Lett.* **125**, 126402 (2020).
- [36] *Electronic Transport in Mesoscopic Systems*, edited by S. Datta (Cambridge University Press, Cambridge, UK, 1995).
- [37] Y.-T. Zhang, X. C. Xie, and Q.-F. Sun, *Phys. Rev. B* **86**, 035447 (2012).
- [38] Y.-T. Zhang, F. Zhai, Z. Qiao, and Q.-F. Sun, *Phys. Rev. B* **86**, 121403(R) (2012).
- [39] W. Long, Q.-F. Sun, and J. Wang, *Phys. Rev. Lett.* **101**, 166806 (2008).
- [40] D. H. Lee and J. D. Joannopoulos, *Phys. Rev. B* **23**, 4997 (1981).
- [41] L. Jin and Z. Song, *Phys. Rev. A* **85**, 012111 (2012).
- [42] M. Znojil, *Phys. Rev. D* **80**, 045009 (2009).